IEEE Access
Multidisciplinary | Rapid Review | Open Access Journal

Received April 14, 2021, accepted May 2, 2021, date of publication May 10, 2021, date of current version May 20, 2021.

Digital Object Identifier 10.1109/ACCESS.2021.3078733

A Generalized Reverse-Electrodialysis Model Incorporating Both Continuous and Recycle Modes for Energy Harvesting From Salinity Gradient Power

ZHIHONG YAN[1], (Student Member, IEEE), YING HUANG[1], (Member, IEEE), CHENXIAO JIANG[2], YING MEI[3], SIEW-CHONG TAN[1], (Senior Member, IEEE), CHUYANG Y. TANG[3], AND SHU YUEN HUI[4,5], (Fellow, IEEE)

[1]Department of Electrical and Electronic Engineering, The University of Hong Kong, Hong Kong
[2]School of Chemistry and Materials Science, University of Science and Technology of China, Hefei 230052, China
[3]Department of Civil Engineering, The University of Hong Kong, Hong Kong
[4]School of Electrical and Electronic Engineering, Nanyang Technological University, Singapore 639798
[5]Department of Electrical and Electronic Engineering, Imperial College London, London SW7 2BX, U.K.

Corresponding author: Ying Huang (yhuang@eee.hku.hk)

This work was supported by the Research Grants Council of the Hong Kong Special Administration Region, China, under Grant C7051-17G.

ABSTRACT Salinity gradient power (SGP) derived from sea and fresh water through reverse electrodialysis (RED) is an emerging discipline with huge potential for carbon-free energy harvesting. SGP technology is still in an infant stage and there is a need for accurate mathematical tools to study its energy harvesting process. Previous models assume a constant salinity gradient with a *continuous* flow of sea water with constant salinity. In the case of *recycling* used sea water, such assumption is no longer valid because the salinity gradient reduces with operating time. This paper presents a generalized RED model that covers both of the continuous and recycle modes. It combines an improved kinetic battery module (KiBaM) with an electrical circuit module (ECM), for capturing the behaviors of both RED stacks operating in continuous mode (C-mode) and those in recycle mode (R-mode). To intuitively describe the compound effects of salinity variation and concentration polarization on electrical performance of the R-mode RED stack, nonlinear capacity effects (i.e., recovery effect and rate capacity effect) and self-consumed effect are introduced into the proposed model. The derivation and extraction procedures of the proposed model are included. An RED stack prototype with 50 pairs of alternating membranes is constructed for model validation. Various pulsed and constant current discharge experimental tests are performed to validate the accuracy of the proposed model.

INDEX TERMS Continuous mode, generalized hybrid model, recycle mode, reverse electrodialysis (RED), salinity gradient power (SGP).

I. INTRODUCTION

Wind and solar energy are the two dominant renewable and carbon-free energy harvesting methods in the power industry [1]. Salinity gradient power (SGP), which is available by mixing two solutions with different salinity, is a kind of renewable energy sources with huge potential but not well explored [2]. This SGP idea is intriguing because the salinity gradient between the oceans and rivers can be considered as a huge renewable energy storage, similar to a large fully charged battery. The global estimated SGP is in the range of 1.4-2.6 TW based on the global discharges of rivers to oceans [3]. This considerable amount of potential power inspires various attempts to develop technologies required for electrical power generation from SGP [4].

Reverse electrodialysis (RED) is an emerging membrane-based technology to harness SGP, featuring the advantage of continuous electricity conversion [5]. In the RED stack,

The associate editor coordinating the review of this manuscript and approving it for publication was Tao Wang.

cation exchange membranes (CEMs) and anion exchange membranes (AEMs) are structured in an alternating pattern between the anode and cathode to form low-salinity solution compartments and high-salinity solution compartments [6]. When the solutions are fed into the stack, the selective transport of cations and anions through the membranes driven by the concentration gradient results in an electrochemical potential, which can be converted into electricity by the redox reaction on the electrodes [7].

Generally, the RED stack operates in either of the two operation modes: 1) continuous mode (C-mode) and 2) recycle mode (R-mode), of which the schematics are shown in Fig. 1 (a) and Fig. 1 (b), respectively. In the C-mode, fresh feed solutions are continuously fed into the compartments [8]. As an analogy of a battery, the constant salinity gradient across the membrane in an RED stack is similar to a constant state-of-charge (*SOC*) in a battery. In the R-mode, the feed solutions are recirculated or recycled in the stack, until the chemical potential is depleted [9]. The equivalent *SOC* will decrease as energy continues to be harvested from the stack. Therefore, an accurate RED stack model for R-mode will automatically cover the C-mode under which the equivalent *SOC* is kept constant. C-mode RED stacks are widely applied in power generation scenes, such as large-scale pilot plants [10], due to their constant power output, while R-mode RED stacks are normally adopted for energy storage applications, such as concentration gradient flow batteries, due to their high energy utilization efficiency, lower costs and longer operation lifetime [11]–[13]. To facilitate the RED stack interfacing with other components such as power electronics circuits and energy storage devices, a high-fidelity model is indispensable [14].

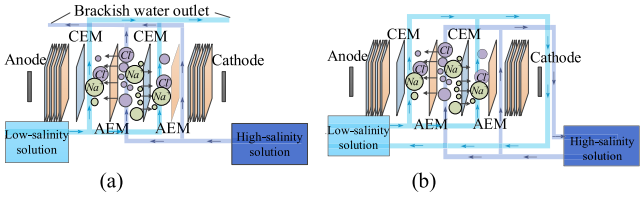

FIGURE 1. An RED stack operating in (a) continuous mode (C-mode) and (b) recycle mode (R-mode).

To date, a variety of electrochemical models have been proposed for RED stacks [15]–[21]. These models can describe the chemical processes taking place in the RED stack [22]. However, establishing these models requires detailed knowledge of the chemical processes and the identification of a range of system parameters [17]. Although there are publications on various modeling approaches of RED stacks, very few of them involve the R-mode operation of the RED stack. In contrast to the time-invariant salinity in the C-mode RED stack, the concentrations of two solutions in the R-mode RED stack significantly change over time and approach the equilibrium concentration finally [21]. This characteristic remarkably complicates the chemical process and poses a barrier for directly applying the existing electrochemical models which are proposed for C-mode RED stacks to R-mode RED stacks.

In Ref. [21], a modified electrochemical model is proposed to describe the concentration variation of an R-mode RED stack, by introducing an operating factor standing for the mixing content of solutions. Nevertheless, an influential phenomenon, i.e. the concentration polarization phenomenon (which has significant effects on reducing the electromotive force over the membrane and introducing additional resistances of the interfacial ionic charge transfer through diffusion boundary layer [24]) is ignored in this model [23]. Moreover, similar to the existing electrochemical models established for C-mode RED stacks [15]–[20], this modified electrochemical model in [21] for the R-mode RED stack is based on constant current (CC) discharge profile, which is inapplicable to other discharge profiles, e.g., pulsed current (PC) discharge profile, as the state transformation of the concentration polarization induced by load-step is not covered. In the PC discharge profile, the concentration polarization is gradually weakening during the idle period between two pulses. It has been proven that the PC discharge profile is effective to alleviate the adverse effects of two essential issues, i.e., concentration polarization and fouling, which contributes to an intensification of electrodialysis [25]. However, to the best of authors' knowledge, there is no publication for RED stack modelling based on PC discharge profile. In summary, although the model work for C-mode RED stacks is fairy matured, the work for R-mode RED stacks especially that with PC discharge profile, is still rare. Extremely complex chemical processes in R-mode RED stacks induced by salinity variation and concentration polarization bring great challenges to the model construction.

In this paper, a generalized hybrid model integrating an improved kinetic battery module (KiBaM) and an electrical circuit module (ECM) is proposed to capture the performance of R-mode RED stacks. It automatically covers the C-mode which is simply one operating condition of this generalized model. This proposed model is able to capture the I-V dynamic characteristics of the RED stack under various discharge profiles, e.g. CC and PC discharge profiles.

To summarize, the main contributions of this paper are:

1. The proposed generalized hybrid model is the first uniform model covering both C-mode and R-mode operations of the RED stack, which are important for its system design.
2. This is the first modelling work for RED stacks covering both constant and pulsed current discharge profile. In addition to describing its electrical characteristics under the constant current discharge profile as most previous models do, the proposed model can also accurately characterize RED stacks' dynamic electrical performance under the pulsed current discharge profile due to its capability to include dynamics of the stack.
3. An improved kinetic battery module is introduced to model chemical processes of the RED stack by a kinetic process with only one-order differential equations.

It simplifies the determination of the parameters in the equivalent circuit of the RED model, which achieves a breakthrough in the study of interfacing RED stacks and other power-electronics-based circuits and energy storage devices. Besides, due to its ease of computation, the model provides an unprecedent opportunity for real-time performance prediction for power management and real-time maximum power tracking implementation of the RED stack.

The rest of the paper is structured as follows. In Section II, the electrical characteristics of R-mode RED stacks are analyzed based on the effects of concentration polarization and salinity variation. Section III describes the proposed generalized hybrid model, corresponding the details of the model to the electrical characteristics stated in Section II. In Section IV, methods of model extraction are provided by using one prototype of the RED stack as an example. In Section V, comparison of simulated and experimental results is presented to validate the proposed model and the reasons for errors are also discussed. Section VI concludes the paper and highlights the contributions of this generalized model for RED stacks.

II. ELECTRICAL CHARACTERISTICS OF R-MODE RED STACKS

In the RED stack, the voltage drop across one ion exchange membrane (IEM), i.e., the trans-membrane potential, can be described according to the Nernst Equation [27]. Based on this equation, a higher concentration difference between two sides of one IEM generally leads to a higher trans-membrane potential, and results in a higher total capacity. In the R-mode RED stack, due to the mass transport by ion diffusion during the circulation of solutions, the concentration of the low-salinity and high-salinity solutions gradually increases and decreases, respectively, which diminishes the concentration difference between them [13]. Thus, the trans-membrane potential will decrease over time domain, resulting in the reduction of the open circuit voltage. Meanwhile, the salinity variation consumes the total capacity of the RED stack.

Theoretically, the total internal resistance of an ideal RED stack is the sum of the resistances of the IEMs, solution resistances and electrode resistance, i.e., resistance of AEMs and CEMs, low-salinity solution, high-salinity solution, anode system, and cathode system. However, in the practical state, with the supply of current, a boundary layer is produced on the interface of the IEM because of the fluid viscous resistance. Take the situation of the boundary layer beside one CEM as an example. As shown in Fig. 2 (a), concentrations distribute nonlinearly in the boundary layer, where the depth of shade represents the concentration level. In the high-salinity solution side, the closer to the membrane surface, the lower the concentration is, while the situation is totally opposite in the low-salinity solution side. This phenomenon is called concentration polarization, which decreases the actual concentration difference between solutions [30]–[34]. As a result, the practical trans-membrane potential is lower than the theoretical value, which leads to a lower open circuit

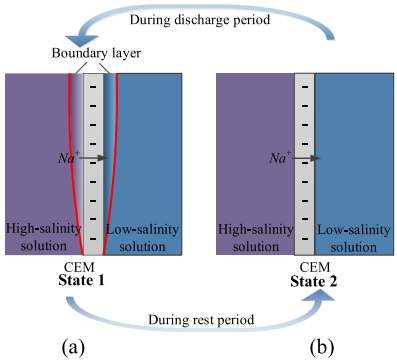

FIGURE 2. The diagram of the concentration polarization in the boundary layer. (a) State 1: under constant current load condition; (b) State 2: under no load condition (The effect of ion free diffusion is insignificant compared to that of electrical-driven diffusion, which is ignored in State 2).

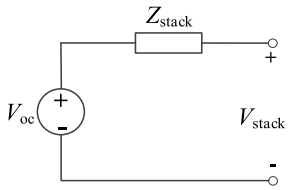

FIGURE 3. Equivalent circuit of the R-mode RED stack.

voltage (V_{oc}) of the stack. This contributes to the earlier arrival of the stack voltage to the cutoff voltage, which implies a less delivered capacity. Meanwhile, concentration polarization increases the total internal resistance of the stack by introducing an additional resistance [35], [36], which also exerts a negative effect on V_{oc}. Moreover, the concentration polarization effect is often exacerbated by a larger discharge current [30] and relieved by a lighter load. Under the CC discharge profile, the boundary layer remains in State 1 (Fig. 2 (a)), while under the PC discharge profile, the boundary layer experiences a gradual transition from State 1 (Fig. 2 (a)) to State 2 (Fig. 2 (b)) during rest period and an inverse transition during discharge period. Under no load condition, concentration polarization can only be induced by the free diffusion, whose effect is almost negligible compared with the effect brought by electrical-driven diffusion.

The equivalent electrical circuit of the R-mode RED stack can be simplified as a voltage source V_{oc} in series with an impedance Z_{stack} as shown in Fig. 3. The electrical characteristics of the RED stack operating in R-mode induced by salinity variation and concentration polarization can be summarized as:

Characteristic (a): V_{oc} decreases over time domain due to the reduction of concentration difference between solutions;

Characteristic (b): The total capacity is lessened over time domain resulting from the salinity variation. This part of consumed capacity is irrecoverable;

Characteristic (c): V_{oc} experiences an extra decrease due to concentration polarization, which will be mitigated by a smaller current;

Characteristic (d): The concentration polarization is insignificant under no load condition, which can be ignored; and

Characteristic (e): The equivalent impedance Z_{stack} is affected by salinity variation and concentration polarization.

III. THE PROPOSED MODEL

Based on the aforementioned characteristics, a generalized hybrid model consisting of an improved KiBaM and an ECM is proposed for the R-mode RED stack as illustrated in Fig. 4. It is capable of capturing the influence of concentration polarization and salinity variation on the electrical performance of the stack in a more intuitive way. In this generalized RED model, nonlinear capacity effects, i.e., rate capacity effect and recovery effect, as well as self-consumed effect are brought in to replace the effects of concentration polarization and salinity variation, respectively.

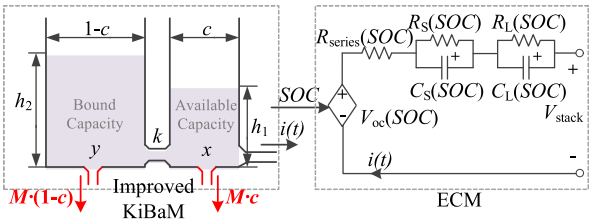

FIGURE 4. A generalized hybrid RED model combining an improved KiBaM with an ECM.

The rate capacity effect refers to the situation that less capacity will be drawn under a larger current condition, while the recovery effect means some previously unavailable capacity turns into available when the load shifts to a lighter one, which leads to a recovery of state of charge (*SOC*). These two effects are inherently correlated. It should be noted that a higher *SOC* in the R-mode RED stack corresponds to a higher open-circuit voltage V_{oc}. Thus, with recovery effect, V_{oc} can be increased under a smaller current due to the recovered *SOC*. This matches *Characteristic* (*c*) in Section II. Self-consumed effect refers to the spontaneous reduction of the total capacity and *SOC* over time domain during the operation of the R-mode RED stack, regardless of whether there are loads connected, which is in accordance with *Characteristic* (*b*) in Section II. Owing to self-consumed effect, open circuit voltage V_{oc} will reduce over time-domain due to the reduced *SOC*. This fits *Characteristic* (*a*) in Section II. As shown in Fig. 4, two outlets are introduced at the bottom of capacity wells in KiBaM to represent self-consumed effect.

In the proposed model, the flow rate ratio of these two outlets is set to a specific value, with the purpose of ensuring zero height difference between bound capacity well and available capacity well under no load condition. Thus, nonlinear capacity effects can be ignored under no load condition as there is no conversion between available capacity and unavailable capacity. Due to the correspondence between nonlinear capacity effects and concentration polarization effect, concentration polarization effect can be neglected in this case. This characteristic of the proposed model conforms *Characteristic* (*d*) in Section II. In the proposed ECM, the equivalent impedance Z_{stack} of the R-mode RED stack is replaced by a series of RC networks. It should be noted that the values of these resistors and capacitors are related to *SOC*, which is determined by the improved KiBaM that reflects nonlinear capacity effects and self-consumed effect. In this way, the relationship between Z_{stack} and nonlinear capacity effects together with self-consumed effect is established. This principle fits *Characteristic* (*e*) in Section II. As a result, the proposed model fits the characteristics of the R-mode RED stack well, of which the details are illustrated in the following sections.

A. IMPROVED KINETIC BATTERY MODULE (KIBAM)

As aforementioned, an improved KiBaM (shown in the left-hand side of Fig. 4) is utilized to capture the RED stack's nonlinear capacity effects [28] and self-consumed effect. An available capacity well and a bound capacity well make up the improved KiBaM [29], [37]. Different from the KiBaM proposed for conventional batteries, both two capacity wells have an outlet representing the self-consumed effect at the bottom, which is shown in Fig. 4 (depicted in red color). The heights and capacities of the available capacity well and the bound capacity well are denoted as h_1 and h_2, and x and y, respectively. The initial total capacity is distributed between two wells at the ratio of c ($0 < c < 1$). The capacity flows from y to x through the valve k whenever there is a height difference between h_1 and h_2. A larger discharge current $i(t)$ will lead to a larger height difference, which implies the nonlinear capacity effects. M represents the flow-out rate of the capacity through two outlets at the bottom of two wells. That is, the self-consumed capacity flows out from two outlets at the rate of $M \cdot c$ and $M \cdot (1-c)$, respectively. Except height variations caused by nonlinear capacity effects, h_1 and h_2 decrease simultaneously due to the self-consumed effect. When h_1 becomes zero, the available capacity is depleted. Consequently, the variations of x and y can be expressed as

$$\begin{cases} \dfrac{dx}{dt} = -i(t) + k\left[h_2(t) - h_1(t)\right] - M \cdot c \\ \dfrac{dy}{dt} = -k\left[h_2(t) - h_1(t)\right] - M \cdot (1-c), \end{cases} \tag{1}$$

where $i(t)$ is the discharge current, $x = c \cdot h_1$ and $y = (1-c) \cdot h_2$. In fact, any discharge process under a time-varying discharge current condition can be divided into several time segments, during which the current is a certain constant value or zero, which is:

$$i(t) = \begin{cases} I, & t_0 < t \le t_d \\ 0, & t_d < t < t_r, \end{cases} \tag{2}$$

where t_0, t_{d} and t_{r} are the initial time, the discharge end time and the end time of the rest period, respectively.

By using Laplace transform and inverse Laplace transform, the solutions of (1) are obtained as

$$\begin{cases} x(t)=x_0e^{-k'(t-t_0)}+\dfrac{(z_0ck'-I-Mc)[1-e^{-k'(t-t_0)}]}{k'} \\ \quad -\dfrac{(I+M)c[k'(t-t_0)-1+e^{-k'(t-t_0)}]}{k'} \\ y(t)=y_0e^{-k'(t-t_0)}+(1-c)z_0[1-e^{-k'(t-t_0)}] \\ \quad -\dfrac{I(1-c)[k'(t-t_0)-1+e^{-k'(t-t_0)}]}{k'}-(1-c)M(t-t_0), \end{cases} \tag{3}$$

where $t_0 < t < t_r, k' = \frac{k}{c(1-c)}$, x_0, y_0 and z_0 are initial conditions of x, y and z, where the relationship among them is determined by $z_0 = x_0 + y_0$.

Thus, the height difference δ(t) between two wells can be expressed as

$$\begin{aligned} \delta(t) &= h_2(t) - h_1(t) = \frac{y(t)}{1-c} - \frac{x(t)}{c} \\ &= \delta(t_0)e^{-k'(t-t_0)} + \frac{I}{c}\cdot\frac{1-e^{-k'(t-t_0)}}{k'}. \end{aligned} \tag{4}$$

The unavailable capacity of the RED stack is

$$C_{\text{unavailable}}(t) = (1-c)\delta(t), \tag{5}$$

and it can be further expressed as:

$$C_{\text{unavailable}}(t) = \begin{cases} C_{\text{unavailable}}(t_0)e^{-k'(t-t_0)}+(1-c)\cdot\dfrac{I}{c}\cdot\dfrac{1-e^{-k'(t-t_0)}}{k'}, \\ \qquad\qquad t_0 < t \le t_d \\ C_{\text{unavailable}}(t_d)e^{-k'(t-t_d)}, \qquad t_d < t < t_r. \end{cases} \tag{6}$$

It shows that the unavailable capacity is irrespective with M, i.e., the symbol of the self-consumed effect.

The relationship among the total capacity C_{total}, the available capacity $C_{\text{available}}(t)$, the unavailable capacity $C_{\text{unavailable}}(t)$, the self-consumed capacity $C_{\text{self-consumed}}(t)$ and the delivered capacity $C_{\text{delivered}}(t)$ can be expressed as:

$$\begin{aligned} C_{\text{available}}(t) = C_{\text{total}} - C_{\text{unavailable}}(t) - C_{\text{self-consumed}}(t) \\ - C_{\text{delivered}}(t), \end{aligned} \tag{7}$$

where $C_{\text{delivered}}(t) = \int i(t)dt$, and $C_{\text{self-consumed}}(t) = \int Mdt$.

Therefore, the SOC of the R-mode RED stack can be calculated as [43]

$$\begin{aligned} SOC(t) = \frac{C_{\text{available}}(t)}{C_{\text{total}}} = SOC_{\text{initial}} \\ - \frac{C_{\text{delivered}}(t) + C_{\text{self-consumed}}(t) + C_{\text{unavailable}}(t)}{C_{\text{total}}}, \end{aligned} \tag{8}$$

where SOC_{initial} is the initial state of SOC.

This improved KiBaM easily and intuitively reflects the nonlinear capacity effects and self-consumed effect of the R-mode RED stack from the view of the kinetic process, which is complex to describe from the view of the chemical process. However, it does not describe the electrical dynamic characteristics of the stack, which brings challenges to RED-driven circuit system design. To solve this issue, an ECM is introduced into the proposed model.

B. ELECTRICAL CIRCUIT MODULE (ECM)

An ECM (shown in the right-hand side of Fig. 4) is integrated to capture electrical dynamic characteristics of the stack. The SOC-controlled voltage source V_{oc} is determined by the real-time SOC obtained from KiBaM. The resistor R_{series} represents the instant discharge energy losses. R_{S} and C_{S}, R_{L} and C_{L} describe the short-term and long-term transient response, respectively. V_{stack} stands for the terminal voltage of the RED stack. Theoretically, in the ECM, V_{oc}, R_{series}, R_{S}, C_{S}, R_{L}, and C_{L} are multivariable functions of the state of charge (SOC), current and temperature. However, for simplicity, these parameters are regarded as single-variable parameters exclusively in relation to the SOC without suffering any significant errors [38]. After observing the curve trends of these parameters versus SOC and learning from the equations adopted in the battery's ECM [39], the combination of exponential functions and polynomial functions is utilized to do the curve fitting of V_{oc}, and exponential functions are used to fit the obtained curves of R_{series} [26], R_{S}, C_{S}, R_{L}, and C_{L}. Therefore, this model is established by the following equation:

$$V_{\text{stack}}(t) = V_{\text{oc}}(SOC) - i(t)\cdot R_{\text{series}} - V_{\text{transient}}(t), \tag{9}$$

$$V_{\text{transient}}(t) = V_{\text{S}}(t) + V_{\text{L}}(t), \tag{10}$$

$$V_{\text{S}}(t) = \begin{cases} R_{\text{S}}(SOC)\cdot i(t)[1-e^{-(t-t_0)/\tau_{\text{S}}}], & t_0 < t \le t_{\text{d}} \\ V_{\text{S}}(t_{\text{d}})\cdot e^{-(t-t_{\text{d}})/\tau_{\text{S}}}, & t_{\text{d}} < t < t_{\text{r}}, \end{cases} \tag{11}$$

$$V_{\text{L}}(t) = \begin{cases} R_{\text{L}}(SOC)\cdot i(t)[1-e^{-(t-t_0)/\tau_{\text{L}}}], & t_0 < t \le t_{\text{d}} \\ V_{\text{L}}(t_{\text{d}})\cdot e^{-(t-t_{\text{d}})/\tau_{\text{L}}}, & t_{\text{d}} < t < t_{\text{r}}, \end{cases} \tag{12}$$

where $\tau_{\text{S}} = R_{\text{S}}(SOC)\cdot C_{\text{S}}(SOC)$, $\tau_{\text{L}} = R_{\text{L}}(SOC)\cdot C_{\text{L}}(SOC)$.

V_{oc} has a relationship with SOC, determined by the combination of exponential functions and polynomial functions, which is

$$V_{\text{oc}}(SOC) = n_0e^{-n_1\cdot SOC} + n_2 + n_3SOC - n_4SOC^2 + n_5SOC^3. \tag{13}$$

The parameters of RC networks are also exponential functions of the SOC, which are derived from

$$\begin{cases} R_{\text{S}}(SOC) = o_0\cdot e^{-o_1\cdot SOC} + o_2\cdot e^{-o_3\cdot SOC} \\ C_{\text{S}}(SOC) = p_0\cdot e^{-p_1\cdot SOC} + p_2\cdot e^{-p_3\cdot SOC} \\ R_{\text{L}}(SOC) = q_0\cdot e^{-q_1\cdot SOC} + q_2\cdot e^{-q_3\cdot SOC} \\ C_{\text{L}}(SOC) = r_0\cdot e^{-r_1\cdot SOC} + r_2\cdot e^{-r_3\cdot SOC} \\ R_{\text{series}}(SOC) = s_0\cdot e^{-s_1\cdot SOC} + s_2, \end{cases} \tag{14}$$

where n_0, n_1, n_2, n_3, n_4, n_5, o_0, o_1, o_2, o_3, p_0, p_1, p_2, p_3, q_0, q_1, q_2, q_3, r_0, r_1, r_2, r_3, s_0, s_1 and s_2 are coefficients to be solved by least-squares fitting tool.

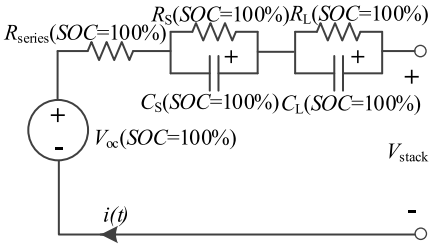

FIGURE 5. The RED model under C-mode operation.

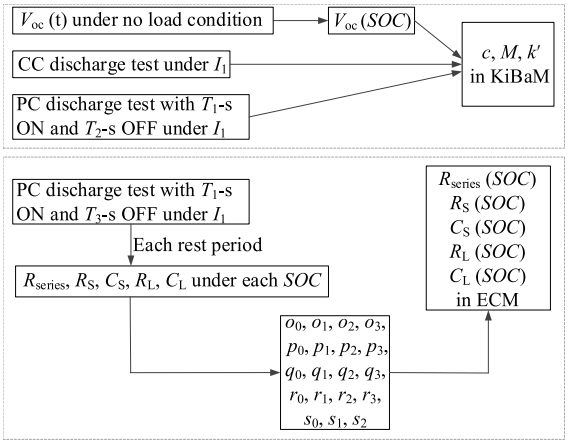

FIGURE 6. Model extraction procedures.

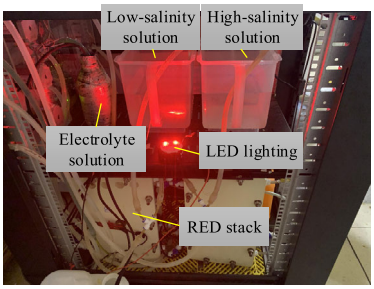

FIGURE 7. The prototype of the RED stack.

TABLE 1. Experimental setup of the RED stack.

Number of AEMs /Pieces	50
Number of CEMs /Pieces	51
Membrane active area per cell /m^2	0.054
Spacer thickness /mm	0.55
Recycled electrolyte solution	$K_3Fe(CN)_6$/ $K_4Fe(CN)_6$
Low-salinity NaCl solution	0.01 mol/L · 8 L
High-salinity NaCl solution	2 mol/L · 6 L
Feed solutions' temperature /K	293
Flow rate /L·s^{-1}	0.008
Cutoff voltage /V	0.5

The C-mode is simply one special operating condition of the R-mode. The time-invariant salinity gradient renders the *SOC* to be constantly 100%. Therefore, V_{oc}, R_{series}, R_S, C_S, R_L and C_L are all constants. In this situation, the generalized RED stack model will be reduced to a simple equivalent circuit model as shown in Fig. 5.

IV. MODEL EXTRACTION

A. FLOW CHART OF MODEL EXTRACTION

The model extraction procedures are detailed in Fig. 6 and illustrated by the following steps.

Step 1: The curve of open circuit voltage V_{oc} versus time is recorded until the cutoff voltage is reached. Along with the variation of the *SOC* obtained from the proposed model in Section III, the curve of V_{oc} (*SOC*) is obtained.

Step 2: One CC discharge test and one PC discharge test where each pulse has T_1-s ON time and T_2-s OFF time, under a same current value I_1, are carried out until the stack voltage reaches the cutoff voltage, during which the voltage curves are both recorded. In this step, a suitable value should be chosen for I_1, which is larger than half of the short-circuit current but smaller than the short-circuit current of the R-mode RED stack so that nonlinear capacity effects are observable. To render the voltage curves during discharge period under two tests close enough, T_2 should be short enough as well as effective for calculation. Step 1 and Step 2 are used to extract the parameters in KiBaM, i.e., c, M and k'.

Step 3: A PC discharge test where each pulse has T_1-s ON time and T_3-s OFF time under I_1 is conducted to extract the parameters of ECM. By fitting the voltage curves of each rest period, *RC* network parameters under different *SOC* values are obtained. Therefore, the relationships between *RC* network parameters and *SOC* can be easily extracted, which construct a complete ECM. Here, T_3 should be long enough to enable the stabilization of V_{oc}. Meanwhile, a longer T_3 will lead to a smaller number of discharge cycles, which may result in insufficient data for parameter extraction. Thus, there should be a trade-off design for T_3.

B. EXAMPLE

A laboratory-scale prototype of an RED stack is constructed for model extraction and validation, as shown in Fig. 7. The dimension of the stack is 250 mm×450 mm×170 mm. The concentrations of the low-salinity solution and the high-salinity solution are chosen respectively as 0.01 mol/L and 2 mol/L in the experiments, representing the salinity of the fresh river water and the brine from seawater desalination plants, respectively. Here, LED is used as a load example of potential industrial applications of the RED technology. Parameters of the experimental setup are provided in Table 1.

1) $V_{oc}(SOC)$-*SOC* CURVE

It is assumed that the total capacity is depleted when the open circuit voltage reaches the pre-set cutoff voltage. $V_{oc}(SOC)$ under no load condition is detected, as shown in Fig. 8, which decreases totally due to the self-consumed effect. During this process, no unavailable capacity is generated since h_1 and h_2 decrease evenly, so there is $C_{total} = C_{self-consumed}$. Therefore,

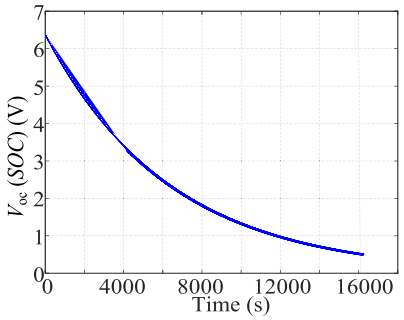

FIGURE 8. Open circuit voltage under no load condition.

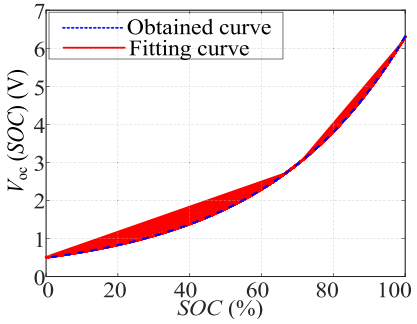

FIGURE 9. $V_{oc}(SOC)$-SOC curve.

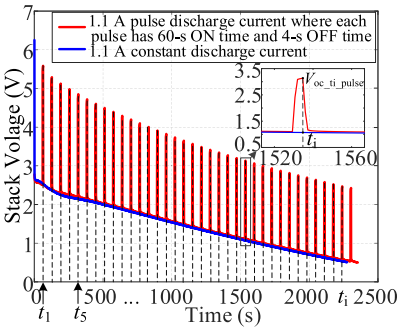

FIGURE 10. Experimental stack voltage V_{stack} under 1.1 A CC discharge condition and 1.1 A PC discharge condition where each pulse has 60-s ON time and 4-s OFF time.

TABLE 2. Model parameters for the RED stack.

n_0	0.516	n_1	6.99	n_2	2.0×10^{-10}	n_3	4.229
n_4	4.918	n_5	6.993	o_0	5.755	o_1	-7.807
o_2	0.0043	o_3	4.588	p_0	899.4	p_1	-5.1×10^{-7}
p_2	-233.9	p_3	1.156	q_0	0.09084	q_1	-0.8888
q_2	0.00029	q_3	5.99	r_0	55.73	r_1	-8.6×10^{-10}
r_2	-0.2816	r_3	4.926	s_0	0.00147	s_1	-6.794
s_2	1.548	c	0.2087	M	1.0031	k'	0.0032

the SOC varying with time can be expressed as

$$SOC(t) = 1 - \frac{M \cdot t}{C_{\text{total}}} = 1 - \frac{M \cdot t}{M \cdot t_{\text{OCV}}} = 1 - \frac{t}{t_{\text{OCV}}}, \quad (15)$$

where t_{OCV} stands for the moment when V_{oc} reaches the cutoff voltage. Thus, $V_{oc}(SOC)$-SOC curve can be obtained as the blue line shown in Fig. 9. The parameters in (13) can be solved by least-squares fitting, of which the results are shown in Table 2 and the curve is shown as the red line in Fig. 9. The RMSE is 0.0069, which implies the fitting accuracy [40].

2) IMPROVED KINETIC BATTERY MODULE EXTRACTION

In our example, I_1 is set as 1.1 A, and T_1 and T_2 are set as 60 s and 4 s, respectively. Therefore, one 1.1 A CC discharge test and one 1.1 A PC discharge test where each pulse has 60-s ON time and 4-s OFF time are conducted to extract the parameters of KiBaM. The experimental results of two tests are shown in Fig. 10. t_{i} ($i = 1, 2, \ldots, N$, where N refers to pulse numbers) is the moment when the rest period comes to the end. Based on (8), $SOC_{\text{constant}}(t_{\text{i}})$ under the 1.1 A CC discharge condition can be rewritten as

$$SOC_{\text{constant}}(t_i) = 1 - \frac{(1.1 + M) \cdot t_i + (1-c) \cdot \frac{1.1}{c} \cdot \frac{1 - e^{-k' t_i}}{k'}}{C_{total}}. \quad (16)$$

Since voltage curves in both discharge periods of CC and PC discharge tests are very close to each other, $SOC_{\text{constant}}(t_{\text{i}}) \approx SOC_{\text{pulse}}(t_{\text{i}})$. $SOC_{\text{pulse}}(t_{\text{i}})$ can be obtained by referring to the $V_{oc}(SOC)$-SOC curve shown in Fig. 9. Therefore, based on (16) and $V_{oc}(SOC)$-SOC curve, c, M and k' are solved by randomly choosing several pulses, of which the results are shown in Table 2.

3) ELECTRICAL CIRCUIT MODULE PARAMETER EXTRACTION

Since T_3 is set as 60 s in our paper, as shown in Fig. 11, the experimental result of one 1.1 A PC discharge test where each pulse has 60-s ON time and 60-s OFF time is used to extract the parameters of ECM. The voltage curve of each rest period is utilized to do parameter extraction, and one of which is zoomed in to show details. According to (9)–(12), the stack voltage during one rest period (bold blue line section in Fig. 11) can be expressed as

$$\begin{aligned} V_{stack}(t) &= o \cdot (1 - e^{-p \cdot t}) + q \cdot (1 - e^{-r \cdot t}) + s \\ &= R_S \cdot I \cdot (1 - e^{-\frac{1}{R_S C_S} t}) + R_L \cdot I \cdot (1 - e^{-\frac{1}{R_L \cdot C_L} \cdot t}) + s, \end{aligned} \quad (17)$$

where $s = V_1$ and R_{S}, C_{S}, R_{L}, and C_{L} are obtained by curve-fitting tool. R_{series} is determined by $R_{\text{series}} = (V_1 - V_0)/I$. Therefore, after obtaining RC network parameters under different SOC values' conditions, the parameters in (14) can be derived by using least-squares fitting, of which the results are shown in Table 2.

V. MODEL VALIDATION AND RESULT ANALYSIS

A. RECYCLE MODE OPERATION

To validate the effectiveness of the proposed model, simulation and experimental tests are carried out, of which the results are compared. Fig. 12 illustrates the implementation

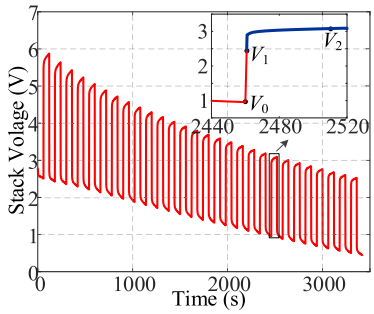

FIGURE 11. Experimental stack voltage V_{stack} under 1.1 A PC discharge condition where each pulse has 60-s ON time and 60-s OFF time (bold blue line refers to the rest period).

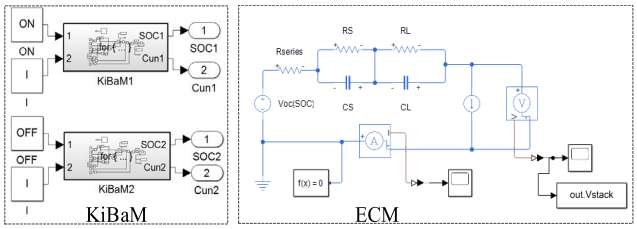

FIGURE 12. The generalized hybrid RED model implemented in MATLAB/Simulink.

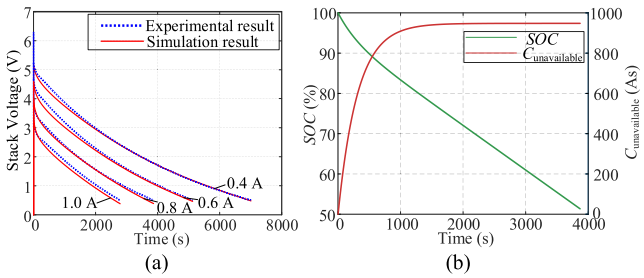

FIGURE 13. (a) Comparison of simulation and experimental results of the stack voltage V_{stack} under 0.4 A, 0.6 A, 0.8 A and 1.0 A CC discharge conditions and (b) *SOC* variation and estimated unavailable capacity under 0.8 A CC discharge condition.

of the proposed generalized hybrid RED model in MATLAB/Simulink. The KiBaM unit yields the *SOC* value, considering the nonlinear capacity effects and self-consumed effect, and then the real-time *SOC* is transferred to the ECM unit, based on which the exact values of RC parameters and the voltage source are given.

The KiBaM unit is made up of two iteration sections, of which the upper one is applicable for non-zero CC discharge conditions, and the lower one suits the rest period (i.e., open circuit condition). Meanwhile, the ECM unit is constructed using components in Simscape toolbox.

The experimental tests are conducted on the RED stack prototype shown in Fig. 7. Fig. 13 (a) shows the comparison between simulated stack voltage curves acquired from the proposed model and the experimental results under 0.4 A, 0.6 A, 0.8 A and 1.0 A CC discharge conditions, respectively (from top to bottom). The voltage errors and runtime errors are all within 5%, which implies acceptable accuracy of the model in capturing the transient voltage response and predicting the runtime under various CC discharge conditions. Fig. 13 (b) shows the simulated *SOC* along with estimated unavailable capacity under 0.8 A CC discharge condition based on the proposed model. Due to the rate capacity effect, $C_{\text{unavailable}}$ firstly increases and then stays unchanged at a relatively high level.

Fig. 14 (a) compares the simulation and experimental results of the stack voltage under 0.9 A PC discharge condition where each pulse has 60-s ON time and 60-s OFF time. The slight difference (within 5% error) between the simulated voltage curve and experimental curve demonstrates that the model precisely predicts the runtime and describes the transient voltage response under a PC discharge condition. The calculation result without considering nonlinear capacity effects is also presented in Fig. 14 (a), which is significantly larger than the experimental result. It indicates the necessity to take nonlinear capacity effects into account since the ignorance of concentration polarization may lead to a higher estimated voltage value, and thus induce the inaccurate estimation of transient voltage response. Fig. 14 (b) presents the simulation result of the *SOC* and the estimated unavailable capacity. It can be seen that $C_{\text{unavailable}}$ increases during the discharge period and then decreases during the rest period, leading to the increase of *SOC* in the rest period accordingly due to the recovery effect.

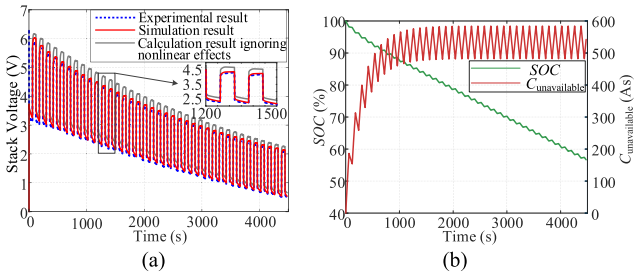

FIGURE 14. (a) Comparison of simulation and experimental results of the stack voltage V_{stack} under 0.9 A PC discharge condition with 60-s ON time and 60-s OFF time and (b) *SOC* variation and estimated unavailable capacity under the same current condition.

Fig. 15 shows the simulated and experimental stack voltage curves under 1.1 A PC discharge condition where each pulse has 60-s ON time and 6-s OFF time. The simulation result matches the experimental result well, which illustrates the validity of the proposed model in capturing the dynamical electrical characteristics under a PC discharge condition with a shorter rest period.

B. CONTINUOUS MODE OPERATION

As aforementioned, the C-mode is simply one special operating condition of the R-mode. As shown in Fig. 5, V_{oc}, R_{series}, R_S, C_S, R_L and C_L are all constants which are derived by substituting *SOC* in (13) and (14) with 100% due to the time-invariant salinity gradient in C-mode. Consequently,

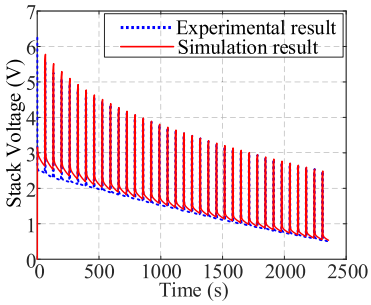

FIGURE 15. Simulated and experimental stack voltage V_{stack} under 1.1 A PC discharge condition where each pulse has 60-s ON time and 6-s OFF time.

TABLE 3. Model parameters for the C-mode stack.

$V_{oc}(SOC{=}100\%)$	6.52 V	$R_{series}(SOC{=}100\%)$	2.86 Ω
$R_S(SOC{=}100\%)$	0.15 Ω	$C_S(SOC{=}100\%)$	16.92 F
$R_L(SOC{=}100\%)$	0.42 Ω	$C_L(SOC{=}100\%)$	156.25 F

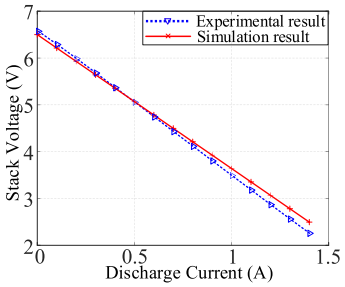

FIGURE 16. Simulated and experimental *V-I* curve of the C-mode RED stack.

the results of V_{oc}, R_{series}, R_S, C_S, R_L and C_L in C-mode are shown in Table 3 for the reduced model shown in Fig. 5.

Fig. 16 shows both the simulated and experimental *V-I* curves plotted for the C-mode RED stack, which are linear lines. The slope of the curve indicates the total resistance $R_{total}(SOC{=}100\%)$ of the C-mode RED stack, where $R_{total}(SOC{=}100\%){=}R_{series}(SOC{=}100\%){+}R_S(SOC{=}100\%){+}R_L(SOC{=}100\%)$. The simulated and experimental values of R_{total} are 3.42 Ω and 3.107 Ω, respectively. The error of the total resistance is around 10%.

Fig. 17 compares the simulation and experimental results of the stack voltage under 1.1 A PC discharge condition where each pulse has 15-s ON time and 40-s OFF time. Errors within 2% imply the accuracy of the reduced RED model under C-mode operation. Fig. 18 shows the simulated and experimental stack voltage curves under 1.2 A PC discharge condition where each pulse has 15-s ON time and 30-s OFF time. The consistency of the two curves illustrate the model's effectiveness in capturing the C-mode stack's electrical performance.

C. ESTIMATED MAXIMUM TOTAL OUTPUT POWER

A maximum power of about 3.5 W has been successfully harvested from the RED stack prototype in this paper, which

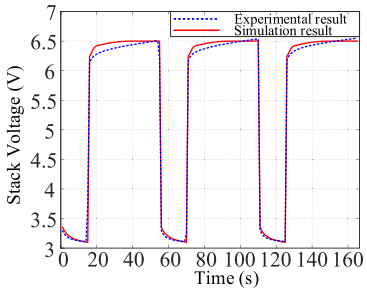

FIGURE 17. Simulated and experimental stack voltage V_{stack} under 1.1 A PC discharge condition where each pulse has 15-s ON time and 40-s OFF time.

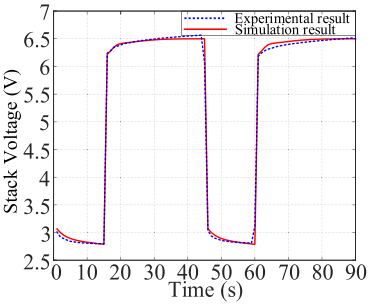

FIGURE 18. Simulated and experimental stack voltage V_{stack} under 1.2 A PC discharge condition where each pulse has 15-s ON time and 30-s OFF time.

owns a volume of 1.91×10^{-2} m^3 (with external dimensions: 25 cm×45 cm×17 cm) and a total membrane active area of 2.7 m^2 at a membrane power density of 1.3 W/m^2. As an estimation, about 3,979 RED stacks of this size can be fitted into a standard 40-ft container box (with internal dimensions of 1204 cm×269 cm ×235 cm). This indicates that a scaled-up version of the RED system of the size of such container box can provide a total power of about 13.9 kW. Since SGP can be continuously harvested and there is a vast storage of it, this estimated figure further signifies the huge potential of the RED technology, particularly when there is much scope for increasing the power density in the membrane discipline.

D. RESULTS DISCUSSION

The errors between simulation results and experimental results mainly come from the following three aspects:

1. Model approximation: The chemical process in the RED stack is too complicated to be represented simply by an extremely accurate model. Thus, a model approximation is normally made to achieve a sufficiently accurate result while reducing the complexity of the model significantly. In this paper, the proposed generalized model considers two of the most significant effects in the stack, which are concentration polarization and salinity variation by means of the improved KiBaM, while ignores some less important effects, such as spacer shadow effect and the influence of the electrolyte solution [41]. Moreover, the quantification of the concentration polarization is difficult, as this involves the complicated

TABLE 4. Comparison of the proposed model and previous models for RED stacks.

Reference	Suitable for C-mode operation	Suitable for R-mode operation	Requires details of chemical processes and vast system parameters	Considers concentration polarization	Based on CC discharge conditions	Based on PC discharge conditions	Implementation complexity	Accuracy
[15]–[17]	Yes	No	Yes	No	Yes	No	High	High
[20]	Yes	No	No	No	Yes	No	Low	High
Proposed	Yes	Yes	No	Yes	Yes	Yes	Low	High

mechanism of the RED stack influenced by multiple factors such as current density, solutions' concentrations, and operating time [42]. In this paper, due to the balance between simplification and accuracy, the influence of current density on the concentration polarization is considered. Hence, the estimation of its effect in this paper may contain some trivial errors.

2. Model parameter approximation: Theoretically, in the electrical circuit model (ECM), the open circuit voltage V_{oc}, the series resistor R_{series}, and RC networks including R_S, C_S, R_L, and C_L are multivariable functions of the state of charge (*SOC*), current and temperature. However, for calculation simplicity, these parameters are regarded as single-variable parameters exclusively in relation to the *SOC* in this paper. Therefore, this simplification may result in some errors between the simulation results and experimental results. Besides, curve fitting is utilized to derive the relationship between V_{oc}, R_{series}, R_S, C_S, R_L, C_L and the *SOC*. Although the fitting accuracy is relatively high, there are slight differences between actual values and fitted values, which also accounts for the errors.

3. Experiment operation error:

(a) Theoretically, the R-mode RED stack starts to be discharged from 100% *SOC*. To reach the 100% *SOC*, before the experiment starts, feed solutions need to be pumped into the stack to fill the compartments, and then it takes some time before the ions can distribute uniformly in the compartments. During this preparation process, the open circuit voltage keeps rising until it stabilizes around a peak point. Due to the random distribution of ions, the time it takes to reach the peak voltage and also the value of the peak voltage differ slightly in each experiment. Therefore, repeating pre-experiments gives a reliable reference value of this peak open circuit voltage, which is used as the symbol of 100% *SOC* and also the starting point of our experiments. However, it is implausible to achieve a perfectly same starting point for each experiment, which renders some deviation of the experimental results. The deviation of the starting point in our experiment is nearly 3%.

(b) Moreover, in our experiments, to exclude the temperature effect, we try to roughly fix the solutions' temperature at a constant value by observing the temperature sensor. The feed solutions' temperature is controlled at (293±1) K. There are still small variations of the temperature in each experiment, which may affect the results.

(c) In addition, small manual errors of the solutions' initial volumes lead to experimental concentration variances, which also influence the results. In our experiment, the volume errors are controlled within 2%.

(d) Furthermore, there are some inevitable minute errors of the concentrations of the feed solutions. For example, although the stack is flushed with clean water after each experiment, due to the large-scale stack, there are still solutions left inside the compartments, which may slightly affect the solution concentration of the subsequent experiment. Moreover, during the recycle of the solutions, ions may not distribute evenly in the large solution tanks, which results in slight deviation of the pumped-in solutions' concentrations from the pre-set value. This contributes to some difference between the anticipated results and experimental results.

E. COMPARISON OF THE PROPOSED MODEL AND PREVIOUS MODELS FOR RED STACKS

To clearly differentiate the advantages of the proposed model over the previous models proposed for RED stacks, their capabilities and degree to describe the performance of the RED stack, as well as their implementation complexity are compared in this section, as shown in Table 4.

VI. CONCLUSION

Based on an improved kinetic battery module (KiBaM) and an electrical circuit module (ECM), a generalized model incorporating both the continuous and recycle modes for RED stacks is presented. The electrical characteristics of the R-mode RED stack illustrated in the proposed model well fit that derived from the analysis of chemical processes. Moreover, this model can be applied to the C-mode, when the *SOC* is constant. When compared with practical measurements, the simulation voltage results obtained from the proposed model have less than 5% error. These results confirm that the model is accurate in tracking the *SOC*, capturing the transient voltage response and predicting the runtime. Because this is an equivalent electrical circuit model, it can be easily adopted into circuit simulation packages to study the interactions of the RED system and the power-electronics-based energy harvesting circuit to perform various maximum power tracking strategies. Compared with wind and solar power, energy harvesting from salinity gradient power is less well explored. It is envisaged that the proposed model can be used by the power electronics research community as a useful tool to study the energy harvesting and storage characteristics of the RED systems.

REFERENCES

[1] K. Strunz, E. Abbasi, and D. N. Huu, "DC microgrid for wind and solar power integration," *IEEE J. Emerg. Sel. Topics Power Electron.*, vol. 2, no. 1, pp. 115–126, Mar. 2014.

[2] F. Giacalone, A. Tamburini, M. Papapetrou, A. Cipollina, and G. Micale, "Reverse electrodialysis: Applications to different case studies," in *Proc. IEEE Int. Conf. Environ. Electr. Eng. IEEE Ind. Commercial Power Syst. Eur. (EEEIC / I&CPS Eur.)*, Jun. 2018, pp. 1–4.

[3] H. Gao, B. Zhang, X. Tong, and Y. Chen, "Monovalent-anion selective and antifouling polyelectrolytes multilayer anion exchange membrane for reverse electrodialysis," *J. Membrane Sci.*, vol. 567, pp. 68–75, Dec. 2018.

[4] G. Z. Ramon, B. J. Feinberg, and E. M. Hoek, "Membrane-based production of salinity-gradient power," *Energy Environ. Sci.*, vol. 4, no. 11, pp. 4423–4434, Jul. 2011.

[5] X. Zhu, T. Kim, M. Rahimi, C. A. Gorski, and B. E. Logan, "Integrating reverse-electrodialysis stacks with flow batteries for improved recovery from salinity gradients and energy storage," *ChemSusChem*, vol. 10, no. 4, pp. 797–803, Feb. 2017.

[6] E. Brauns, "Salinity gradient power by reverse electrodialysis: Effect of model parameters on electrical power output," *Desalination*, vol. 237, nos. 1–3, pp. 378–391, Feb. 2009.

[7] B. E. Logan and M. Elimelech, "Membrane-based processes for sustainable power generation using water," *Nature*, vol. 488, no. 7411, pp. 313–319, Aug. 2012.

[8] L. Gurreri, G. Battaglia, A. Tamburini, A. Cipollina, G. Micale, and M. Ciofalo, "Multi-physical modelling of reverse electrodialysis," *Desalination*, vol. 423, pp. 52–64, Dec. 2017.

[9] E. Mercer, C. J. Davey, D. Azzini, A. L. Eusebi, R. Tierney, L. Williams, Y. Jiang, A. Parker, A. Kolios, S. Tyrrel, E. Cartmell, M. Pidou, and E. J. McAdam, "Hybrid membrane distillation reverse electrodialysis configuration for water and energy recovery from human urine: An opportunity for off-grid decentralised sanitation," *J. Membrane Sci.*, vol. 584, pp. 343–352, Aug. 2019.

[10] M. Tedesco, A. Cipollina, A. Tamburini, and G. Micale, "Towards 1 kW power production in a reverse electrodialysis pilot plant with saline waters and concentrated brines," *J. Membrane Sci.*, vol. 522, pp. 226–236, Jan. 2017.

[11] W. J. van Egmond, U. K. Starke, M. Saakes, C. J. N. Buisman, and H. V. M. Hamelers, "Energy efficiency of a concentration gradient flow battery at elevated temperatures," *J. Power Sources*, vol. 340, pp. 71–79, Feb. 2017.

[12] W. J. van Egmond, M. Saakes, S. Porada, T. Meuwissen, C. J. N. Buisman, and H. V. M. Hamelers, "The concentration gradient flow battery as electricity storage system: Technology potential and energy dissipation," *J. Power Sources*, vol. 325, pp. 129–139, Sep. 2016.

[13] R. S. Kingsbury, K. Chu, and O. Coronell, "Energy storage by reversible electrodialysis: The concentration battery," *J. Membrane Sci.*, vol. 495, pp. 502–516, Dec. 2015.

[14] J. Veerman, J. W. Post, M. Saakes, S. J. Metz, and G. J. Harmsen, "Reducing power losses caused by ionic shortcut currents in reverse electrodialysis stacks by a validated model," *J. Membrane Sci.*, vol. 310, nos. 1–2, pp. 418–430, Mar. 2008.

[15] D. H. Kim, B. H. Park, K. Kwon, L. Li, and D. Kim, "Modeling of power generation with thermolytic reverse electrodialysis for low-grade waste heat recovery," *Appl. Energy*, vol. 189, pp. 201–210, Mar. 2017.

[16] R. Long, B. Li, Z. Liu, and W. Liu, "Reverse electrodialysis: Modelling and performance analysis based on multi-objective optimization," *Energy*, vol. 151, pp. 1–10, May 2018.

[17] J. Veerman, M. Saakes, S. J. Metz, and G. J. Harmsen, "Reverse electrodialysis: A validated process model for design and optimization," *Chem. Eng. J.*, vol. 166, no. 1, pp. 256–268, Jan. 2011.

[18] Y. Mei and C. Y. Tang, "Recent developments and future perspectives of reverse electrodialysis technology: A review," *Desalination*, vol. 425, pp. 156–174, Jan. 2018.

[19] A. A. Moya, "A numerical comparison of optimal load and internal resistances in ion-exchange membrane systems under reverse electrodialysis conditions," *Desalination*, vol. 392, pp. 25–33, Aug. 2016.

[20] Y. Huang, Y. Mei, S. Xiong, S.-C. Tan, C. Y. Tang, and S. Y. Hui, "Reverse electrodialysis energy harvesting system using high-gain step-up DC/DC converter," *IEEE Trans. Sustain. Energy*, vol. 9, no. 4, pp. 1578–1587, Oct. 2018.

[21] W. Li, W. B. Krantz, E. R. Cornelissen, J. W. Post, A. R. D. Verliefde, and C. Y. Tang, "A novel hybrid process of reverse electrodialysis and reverse osmosis for low energy seawater desalination and brine management," *Appl. Energy*, vol. 104, pp. 592–602, Apr. 2013.

[22] J. G. Hong, W. Zhang, J. Luo, and Y. Chen, "Modeling of power generation from the mixing of simulated saline and freshwater with a reverse electrodialysis system: The effect of monovalent and multivalent ions," *Appl. Energy*, vol. 110, pp. 201–210, Oct. 2013.

[23] P. Długołęcki, A. Gambier, K. Nijmeijer, and M. Wessling, "Practical potential of reverse electrodialysis as process for sustainable energy generation," *Environ. Sci. Technol.*, vol. 43, no. 17, pp. 6888–6894, Sep. 2009.

[24] P. Długołęcki, P. Ogonowski, S. J. Metz, M. Saakes, K. Nijmeijer, and M. Wessling, "On the resistances of membrane, diffusion boundary layer and double layer in ion exchange membrane transport," *J. Membrane Sci.*, vol. 349, nos. 1–2, pp. 369–379, Mar. 2010.

[25] Z. He, X. Gao, Y. Zhang, Y. Wang, and J. Wang, "Revised spacer design to improve hydrodynamics and anti-fouling behavior in reverse electrodialysis processes," *Desalination Water Treatment*, vol. 57, no. 58, pp. 28176–28186, Dec. 2016.

[26] J. Zhang, S. Ci, H. Sharif, and M. Alahmad, "Modeling discharge behavior of multicell battery," *IEEE Trans. Energy Convers.*, vol. 25, no. 4, pp. 1133–1141, Dec. 2010.

[27] E. Güler, R. Elizen, D. A. Vermaas, M. Saakes, and K. Nijmeijer, "Performance-determining membrane properties in reverse electrodialysis," *J. Membrane Sci.*, vol. 446, pp. 266–276, Nov. 2013.

[28] T. Kim, W. Qiao, and L. Qu, "An enhanced hybrid battery model," *IEEE Trans. Energy Convers.*, vol. 34, no. 4, pp. 1848–1858, Dec. 2019.

[29] T. Kim and W. Qiao, "A hybrid battery model capable of capturing dynamic circuit characteristics and nonlinear capacity effects," *IEEE Trans. Energy Convers.*, vol. 26, no. 4, pp. 1172–1180, Dec. 2011.

[30] L. Gurreri, A. Tamburini, A. Cipollina, G. Micale, and M. Ciofalo, "Flow and mass transfer in spacer-filled channels for reverse electrodialysis: A CFD parametrical study," *J. Membrane Sci.*, vol. 497, pp. 300–317, Jan. 2016.

[31] P. A. Sosa-Fernandez, J. W. Post, M. S. Ramdlan, F. A. M. Leermakers, H. Bruning, and H. H. M. Rijnaarts, "Improving the performance of polymer-flooding produced water electrodialysis through the application of pulsed electric field," *Desalination*, vol. 484, Jun. 2020, Art. no. 114424.

[32] Q. Gao, Z. Li, C. Lei, R. Fu, W. Wang, Q. Li, and Z. Liu, "Application of pulsed electric field in antifouling treatment of sodium gluconate mother liquor by electrodialysis," *Materials*, vol. 13, no. 11, p. 2501, May 2020.

[33] G. Dufton, S. Mikhaylin, S. Gaaloul, and L. Bazinet, "Systematic study of the impact of pulsed electric field parameters (pulse/pause duration and frequency) on ED performances during acid whey treatment," *Membranes*, vol. 10, no. 1, p. 14, Jan. 2020.

[34] D. Butylskii, I. Moroz, K. Tsygurina, and S. Mareev, "Effect of surface inhomogeneity of ion-exchange membranes on the mass transfer efficiency in pulsed electric field modes," *Membranes*, vol. 10, no. 3, p. 40, Mar. 2020.

[35] J.-H. Choi, J.-S. Park, and S.-H. Moon, "Direct measurement of concentration distribution within the boundary layer of an ion-exchange membrane," *J. Colloid Interface Sci.*, vol. 251, no. 2, pp. 311–317, Jul. 2002.

[36] J. G. Hong, B. Zhang, S. Glabman, N. Uzal, X. Dou, H. Zhang, X. Wei, and Y. Chen, "Potential ion exchange membranes and system performance in reverse electrodialysis for power generation: A review," *J. Membrane Sci.*, vol. 486, pp. 71–88, Jul. 2015.

[37] M. Chen and G. A. Rincon-Mora, "Accurate electrical battery model capable of predicting runtime and I–V performance," *IEEE Trans. Energy Convers.*, vol. 21, no. 2, pp. 504–511, Jun. 2006.

[38] R. C. Kroeze and P. T. Krein, "Electrical battery model for use in dynamic electric vehicle simulations," in *Proc. IEEE Power Electron. Spec. Conf.*, Jun. 2008, pp. 1336–1342.

[39] J. Zhang, S. Ci, Sharif, and M. Alahmad, "An enhanced circuit-based model for single-cell battery," in *Proc. Appl. Power Electron. Conf. Expo.*, Palm Springs, CA, USA, Feb. 2010, pp. 672–675.

[40] R. Ahmed, M. El Sayed, I. Arasaratnam, J. Tjong, and S. Habibi, "Reduced-order electrochemical model parameters identification and state of charge estimation for healthy and aged li-ion batteries—Part II: Aged battery model and state of charge estimation," *IEEE J. Emerg. Sel. Topics Power Electron.*, vol. 2, no. 3, pp. 678–690, Sep. 2014.

[41] J. Liu, G. M. Geise, X. Luo, H. Hou, F. Zhang, Y. Feng, M. A. Hickner, and B. E. Logan, "Patterned ion exchange membranes for improved power production in microbial reverse-electrodialysis cells," *J. Power Sources*, vol. 271, pp. 437–443, Dec. 2014.
[42] L. Gurreri, A. Tamburini, A. Cipollina, G. Micale, and M. Ciofalo, "CFD prediction of concentration polarization phenomena in spacer-filled channels for reverse electrodialysis," *J. Membrane Sci.*, vol. 468, pp. 133–148, Oct. 2014.
[43] C. Liu, X. Cai, and Q. Chen, "Self-adaptation control of second-life battery energy storage system based on cascaded H-Bridge converter," *IEEE J. Emerg. Sel. Topics Power Electron.*, vol. 8, no. 2, pp. 1428–1441, Jun. 2020.

ZHIHONG YAN (Student Member, IEEE) received the B.Eng. degree in electrical engineering from Wuhan University, Wuhan, China, in 2019. She is currently pursuing the Ph.D. degree with the Department of Electrical and Electronics Engineering, The University of Hong Kong, Hong Kong. Her current research interests include the modeling of reverse electrodialysis stacks and energy harvesting from salinity gradient power and maximum power tracking of renewable energy applications.

YING HUANG (Member, IEEE) received the B.Eng. degree in electrical engineering from Wuhan University, Wuhan, China, in 2013, and the Ph.D. degree in electrical and electronic engineering from The University of the Hong Kong, Hong Kong, in 2018. From March 2014 to August 2014, she was a Research Assistant with the Department of Electrical and Electronic Engineering, The University of Hong Kong. She is currently a Postdoctoral Fellow with the Department of Electrical and Electronic Engineering, The University of Hong Kong. Her current research interests include switched-capacitor converter, resonant converter, wireless power transfer, and renewable energy applications. She was a recipient of the Best Paper Award at the 8th Annual IEEE Energy Conversion Congress and Exposition (IEEE ECCE 2016).

CHENXIAO JIANG received the Ph.D. degree in chemical engineering from the University of Science and Technology of China, in 2016. From 2016 to 2019, he was a Postdoctoral Staff Member with USTC and The University of Hong Kong, from 2019 to 2020. He is currently an Associate Professor with the University of Science and Technology of China (USTC). He has published more than 40 articles on the peer reviewed journals, contributed three book chapters, and hold seven authorized patent. His research interests include ion exchange membranes and the related processes, such as electrodialysis (ED), reverse electrodialysis (RED), bipolar membrane electrodialysis (BMED), selectrodialysis (SED), and the corresponding applications in seawater desalination, the wastewater treatment, the energy conversion and storage, and the chemical molecule separation.

YING MEI received the M.Eng. degree in environmental engineering from Beijing Normal University, Beijing, China, in 2014, and the Ph.D. degree in civil engineering from The University of Hong Kong, Hong Kong, in 2019. She was a Postdoctoral Research Fellow in civil engineering with The University of Hong Kong, from September 2019 to August 2020. She is currently an Associate Professor with the Advanced Institute of Natural Sciences of Beijing Normal University, Zhuhai, China. Her research interests include membrane technology, waste water management, desalination, and clean energy.

SIEW-CHONG TAN (Senior Member, IEEE) received the B.Eng. (Hons.) and M.Eng. degrees in electrical and computer engineering from the National University of Singapore, Singapore, in 2000 and 2002, respectively, and the Ph.D. degree in electronic and information engineering from The Hong Kong Polytechnic University, Hong Kong, in 2005.

He was a Visiting Scholar with the Grainger Center for Electric Machinery and Electromechanics, University of Illinois at Urbana-Champaign, Champaign, from September to October 2009. He was an Invited Academic Visitor with the Huazhong University of Science and Technology, Wuhan, China, in December 2011. He is currently a Professor with the Department of Electrical and Electronic Engineering, The University of Hong Kong, Hong Kong. He is a coauthor of the book *Sliding Mode Control of Switching Power Converters: Techniques and Implementation* (Boca Raton: CRC, 2011). His research interests include power electronics and control, LED lightings, smart grids, and clean energy technologies.

Dr. Tan serves as an Associate Editor of the IEEE TRANSACTIONS ON POWER ELECTRONICS.

CHUYANG Y. TANG is currently a Professor of environmental engineering with The University of Hong Kong. He is also an Inventor of aquaporin-based biomimetic membranes. He has published more than 200 peer reviewed publications. His research interests include membrane technology for water and energy applications. He was a recipient of the Hong Kong RGC Senior Research Fellowship, the Finland Distinguished Professor Program Fellowship, and the International Desalination Association Fellowship.

SHU YUEN (RON) HUI (Fellow, IEEE) received the B.Sc.Eng. (Hons.) degree in electrical and electronic engineering from the University of Birmingham, Birmingham, U.K., in 1984, and the D.I.C. and Ph.D. degrees from Imperial College London, London, U.K., in 1987.

He is concurrently the MediaTek Endowed Professor with the School of Electrical and Electronic Engineering, Nanyang Technological University, Singapore, and a part-time Chair Professor of power electronics with Imperial College London. He has published more than 300 refereed journal publications and book chapters, and more than 60 of his patents have been adopted by industry.

Dr. Hui is a Fellow of the Australian Academy of Technological Sciences and Engineering, the US National Academy of Inventors, and also the Royal Academy of Engineering, U.K. He was a recipient of the 2010 IEEE Rodulf Chope Research and Development Award, the 2010 IET Crompton Medal, and the 2015 IEEE William E. Newell Power Electronics Award. He is currently an Associate Editor of the IEEE TRANSACTIONS ON POWER ELECTRONICS. He is also an Editor of the IEEE JOURNAL OF EMERGING AND SELECTED TOPICS IN POWER ELECTRONICS.